Aerosol Science and Engineering (2021) 5:460–477
https://doi.org/10.1007/s41810-021-00115-4

ORIGINAL PAPER

Analysis of Positive and Negative Atmospheric Air Ions During New Particle Formation (NPF) Events over Urban City of India

Jeni Victor Nepolian[1] · Devendraa Siingh[1] · R. P. Singh[2] · Alok Sagar Gautam[3] · Sneha Gautam[4]

Received: 18 June 2021 / Revised: 22 July 2021 / Accepted: 25 July 2021 / Published online: 9 August 2021

Abstract

Simultaneous measurements of ion-mobility spectra of both polarities with a Neutral Air Ion Spectrometer (NAIS) operating in the mobility range 3.16–0.00133 $cm^2\ V^{-1}\ s^{-1}$ (mass diameter range 0.36–47.1 nm) and concentration of Radon (^{222}Rn) were carried out at Pune (18° 31′ N, 73° 55′ E, 560 m above mean sea level). ^{222}Rn progenies measured by a Radon detector, RTM 2200, and surface meteorological parameters during the period January 2012 to December 2012 were analysed. During this period, NPF events were observed on 28 days and 222 days were without any event (non-event). NPF events mostly occurred by photochemistry in the morning hours of the pre-monsoon season (~ 62%) during the hottest months (April and May) of the year. Authors studied different features of new particle formation (NPF) events, and their dependence on meteorological parameters. The annual mean diurnal variations of different categories of ions show a primary maximum in the morning hour along with the secondary maxima in the evening hour and a minimum in the afternoon. The results are explained in terms of the atmospheric boundary layer changes and katabatic wind blowing along the hill slope surrounded by the measurement site. The computed ion production rate correlates (correlation coefficient $R = 0.67$) well with the observed small cluster ions. Also, the role of temperature and humidity on the ion concentration on both for the event and non-event days are discussed. Using the principal component analysis (PCA), the first five principal components were found to represent more than 98% of the total variance on event and non-event days. Even the first principal component explained about ~ 86% (65%) of the total variance on non-event (event) days. The statistical analysis also confirms that the small and large—ions on non-event days originated from a similar physical/chemical background.

Keywords New particle formation · Ion-mobility spectra · Principle component analysis · Ionization rate · Radon

1 Introduction

The presence of ions in the atmosphere is the resultant balance between the ion production rate and loss of ions through different processes. In the lower atmosphere/troposphere, cosmic rays are the primary source of ionization and are the main source of ionization above a height of ~ 1 km (Hoppel et al. 1986; Carslaw et al. 2002; Siingh and Singh 2010; Singh et al. 2011; Kumar et al. 2018). Geomagnetic fields influence the movement of cosmic rays in the Earth's environment; hence ionization produced in the atmosphere is dependent on geomagnetic latitude and solar variability. However, near the Earth's surface, the source of ionization is dominantly radioactive radiations and their daughter products. Bricard (1965) estimated the relative contributions of ion production rates from air, soil and cosmic origins to be 4.5, 3.5 and 2 ion-pairs $cm^{-3}\ s^{-1}$, respectively in continental regions. In the tropical zone near the Earth's

✉ Devendraa Siingh
devendraasiingh@tropmet.res.in

✉ Alok Sagar Gautam
phyalok@gmail.com

✉ Sneha Gautam
snehagautam@karunya.edu; gautamsneha@gmail.com

[1] Indian Institute of Tropical Meteorology, Ministry of Earth Sciences, New Delhi, Dr Homi Bhabha Road, Pashan, Pune 41100, India

[2] Department of Physics, Banaras Hindu University, Varanasi 221005, India

[3] Department of Physics, HNB Garhwal University, Srinagar 246174, India

[4] Department of Civil Engineering, Karunya Institute of Technology and Sciences, Coimbatore 641114, Tamil Nadu, India

surface, ionization processes are controlled by Radon and its progenies (Hensen and van der Hage 1994). In addition, several other natural sources of small ions production near the ground are corona ions produced in large electric fields, splashing of rain drops at the ground, breaking of water droplets near to the waterfalls and sea shores, dust storms, volcanoes, etc., (Chalmers 1967; Blanchard 1963; Siingh et al. 2005; Horrak et al. 2006; Kolarz et al. 2012; Kamra et al. 2015a). The mechanism responsible for the production of charge and the nature of atmospheric air ions distributions shows that temporal and spatial variations are not well understood.

Atmospheric air ions play a primary role in the discipline of atmosphere electricity because their motion in the atmosphere determines the air conductivity and air-earth current (Wilson 1924; Siingh et al. 2007a). In recent decades, the area of study has become more attractive because ions are actively involved in the formation of secondary aerosol particles (Hoppel 1985; Yu and Turco 2000; Kulmala et al. 2004; Gopalakrishnan et al. 2005; Yu 2010; Siingh et al. 2013a; Tammet et al. 2014) and as such these ions are found to influence the quality of air and climate system (Waring et al. 2011). Air ions consist of charged particles of diverse chemical compositions. They grow from molecular clusters to large aerosol particles and attain a characteristic distribution in mass and size (Tammet 1998). The molecular clusters behave like kernels of condensation of nucleating vapors, converting them from the gas into aerosol particles. The balancing nature of ions is manifested in the atmosphere in many processes, including the balance between cluster ions and aerosol particles via ion-aerosol attachment and the balance between neutral and charged aerosols (charging state of aerosol particles).

It is essential to understand the mechanism of the growth of the newly formed particles to the size of cloud condensation nuclei and cloud processes under different environmental conditions to estimate the radiative forcing on the regional and global scales (Kulmala et al. 2004; Sullivan et al. 2018; Gautam et al. 2021). Observations to investigate the formation and growth of ultrafine particles have been made under a variety of environmental conditions (Kulmala et al. 2004, 2013, 2007b, 2011, 2018; Siingh et al. 2005; Tammet et al. 2006; Qian et al. 2007; Asmi et al. 2010; Betha et al. 2013; Kanawade et al. 2014; Kamra et al. 2015b; Huang et al. 2016; Dinoi et al. 2021; Gautam and Brema 2020; Gollakota et al. 2021; Ambade et al. 2021). Even though the physical/chemical process involved is not clearly understood, much more measurements under varying conditions are required.

Several mechanisms of NPF have been proposed such as homogeneous ternary nucleation (Kulmala et al. 2013), ion nucleation cluster (Kanawade and Tripathi 2006; Yu et al. 2008, 2010; Yu and Turco 2011; Gonser et al. 2014), activation of neutral clusters (Kulmala and Lehtinen 2006and nucleation mechanism involving organic vapors (O'Dowd et al. 2002a) or iodine (O'Dowd et al. 2002b). Yu (2010) based on a the kinetic model of ion-mediated nucleation mechanism showed that the nucleation rate nonlinearly depends on sulphuric acid vapour concentration, temperature, and relative humidity ionization rate and surface area of existing particles. The studies involving kinetic model of ion-mediated nucleation showed that this process can explain the rapid initial growth of small clusters to a size of ~ 1.5 nm diameter by charge-neutral interactions (Yu and Turco 2001, 2008; Yu 2007, 2010). The measurements of Kamra et al. (2015b) support the theory of formation and growth of ions below the inversion layer by the ion-mediated nucleation mechanism and /or advection of ion with katabatic winds during the period of enhanced concentration of ions and aerosols when the solar radiation is absent or very low in the early morning hours.

Commonly used atmospheric electrical parameters are air conductivity, small ion concentration and heavy large ion concentration (Cobb 1977; Siingh et al., 2005). In the constant ionization rate, the concentration of small ions is inversely proportional to the diameter of concentrated aerosol particles (Salm et al. 1992; Horrak 2001). The concentration of heavy large ions is related to the content of Aitken aerosol particles (30–80 nm) in the air at the measurement site. The relation between the ion concentration and meteorological factors was primarily indirect, caused by the variation of ionization rate and aerosol particle content in air. The mobility of small air ions decreased by about 20% with increasing temperature from −5 to 25 °C (Salm et al. 1992) and is also influenced by the direction of wind blowing at the time and place of observation. The mean mobility of small air ions is an essential factor that can affect the conductivity of atmospheric air to a large extent. The deviation of mean mobility from the average value could cause changes in conductivity (induced by small ions) from about −12 to 15% and from −14 to 26% for positive and negative polarity, respectively (Siingh et al. 2005).

We carried out the ions measurement using NAIS for the year 2010–2012 at the same measurement site. We reported the few characterizations viz the monthly, seasonal, and annual distribution of air ions (Gautam et al. 2017), NPF events from trace gases (Siingh et al. 2013b) and case studies including rain-induced events (Kamra et al. 2015a, b). In all these studies, diurnal variation was not discussed both for event and non-event days. Therefore, in the present study, the diurnal variations of different categories of air ions during the event and non-event days for the year 2012 are presented. The ion production rate was calculated for both event and non-event days. Results are discussed in terms of change in Radon concentration and its dependencies on the surface stability parameters temperature and humidity.

Polar air conductivity derived on event and non-events days from mobility-conductivity relation is discussed on clustering, aerosol concentration, and contribution of air ions to the total conductivity. Principal component analysis was carried out for a fraction of ions. The best-fitted components were explained by the characteristics of different ions during NPF and non-event days.

2 Data and Analysis

In the lower terrestrial atmosphere in the altitude range of 1 km above the Earth's surface, radioactive gas ^{222}Rn and its progeny. Therefore, simultaneous measurements of ion and Radon were carried out in the premises of Indian Institute of Tropical Meteorology, Pune (18° 31′ N, 73° 55′ E, 560 m above mean sea level), India, which is located in a valley surrounded by 500–800 m high hills on three sides. NAIS uses two unipolar corona dischargers to charge the sampled particles and for their subsequent detection. It has two identical cylindrical aspiration-type differential mobility analyzers (DMA), one for positive ions and another for negative ions. More details on instruments can be found elsewhere Mirme and Mirme (2013), Siingh et al. (2013b) and Kamra et al. (2015b).

NAIS post-processed the measured air ion concentration in the mobility domain (3.16–0.00133 cm^2 V^{-1} s^{-1} mass diameter range 0.36–47.1 nm$^{@}$). ($^{@}$Henceforth, "diameter" should be read as "mass diameter" unless stated otherwise) into number sizes distribution (Mirme and Mirme 2013), which was subsequently converted to the diameter-based mobility distribution using size conversion model of Tammet (1995). The uncertainty in the air ion concentration measurements is < 10%. The data are used in quantitative ion cluster studies and accurate determination of formation and growth rates of the particles (Wagner et al. 2016). An average mobility for positive and negative ions is obtained in 5 min, based on 200-s sample air and 100-s offset-level measurements. The entire mobility distribution of the atmospheric ions are divided into two main classes, (1) cluster ions (mobility > 0.5 cm^2 V^{-1} s^{-1}; diameter < 1.6 nm) and (2) charged nanoparticles (mobility < 0.5 cm^2 V^{-1} s^{-1}; diameter > 1.6 nm) (Horrak et al. 2003). These two classes of ions have been further divided into five independent categories based on their size and mobility, viz, small cluster ions (mobility 3.2–1.3 cm^2 V^{-1} s^{-1}, size 0.36–0.85 nm diameter), big cluster ions (mobility 1.3–0.5 cm^2 V^{-1} s^{-1}, size 0.85–1.6 nm diameter), intermediate ions (mobility 0.5–0.034 cm^2 V^{-1} s^{-1}, size 1.6–7.4 nm diameter), light large ions (mobility 0.034–0.0042 cm^2 V^{-1} s^{-1}, size 7.4–22 nm diameter) and heavy large ions (mobility 0.0042–0.00133 cm^2 V^{-1} s^{-1}, 22–47.1 nm diameter) (Mirme and Mirme 2013).

The ion concentrations in the atmosphere show a diurnal and seasonal variation, which are explained in terms of solar irradiance, temperature, humidity, and wind velocity (Kamra et al. 2015b; Gautam et al. 2017). These meteorological parameters are taken from an automatic weather station (AWS) system installed at India Meteorological Department (IMD) campus, ~ 200 m away from the measurements site. At this site, there is a sizeable significant temperature variation with the minimum surface temperature (8–10 °C) during the winter months (December–January) and the maximum temperature often exceeding 40 °C during the pre-monsoon months (April–May). Relative humidity varies 40, 55, 70% in pre-monsoon, winter and post-monsoon, respectively, often exceeds 90% in the monsoon season. Winds were persistently southwesterly during the monsoon season and were comparatively low and changed directions in other seasons.

Radon and its daughter progeny concentrations were measured by Radon detector (RTM 2200 of SARAD GmbH, Germany) from January to December 2012. Details of measurement technique are given in Victor et al. (2019). The inter comparison of small ions derived from ^{222}Rn detector and observed from NAIS has been shown in detail by Singh et al. (2013b) and Gautam (2017).

Ion-pair production depends on the ions-aerosol attachments and ion-ion recombination rate. The same has been calculated using the following equation (Hoppel and Frick 1986).

$$q = \alpha n^2 + n \int \beta\delta(r) z(r) \mathrm{d}r \tag{1}$$

where, q is the ionization rate, $z(r)$ is the particle size distribution (cm^{-3}), n is the concentration of small ions (0.36–1.6 nm, diameter), α is the ion–ion recombination coefficient = 1.6×10^{-6} cm^3 s^{-1}, $\beta\delta = 0.436\ r\ 9.2 \times 10^{-8}$ is the single size attachment coefficient for small ions.

^{222}Rn and its decay in associated with the release of energy which may produce ionization. Concentrations of ^{222}Rn and its progeny were used to estimate total energy released, which was used in the ion-pair production. The ionization rate was then estimated from $Q = \varepsilon/I$, where ε is the total energy, I is the ionization energy (32 eV) required to produce one ion-pair in the atmosphere. The total energy ε is given by Green et al. (1977), Laakso et al. (2004), and Chen et al. (2016a),

$$\varepsilon = 5.49 \times 10^6 \left(C_{222\mathrm{Rn}}\right) + 6 \times 10^6 \left(C_{218\mathrm{Po}}\right) + 7.68 \times 10^6 \left(C_{214\mathrm{Po}}\right) + 0.85 \times 10^6 \left(C_{214\mathrm{Bi}}\right) (\mathrm{eV}) \tag{2}$$

$C_{222\mathrm{Rn}}$, $C_{218\mathrm{Po}}$, $C_{214\mathrm{Po}}$, and $C_{214\mathrm{Bi}}$ are the concentrations of Radon and its progenies (in Bq m^{-3}). In this process, the role of aerosols present in the atmosphere was not considered.

The spectral boundary for different sizes (small, intermediate, and large) of ions can be more precisely defined using principal component analysis (PCA) (Horrak et al. 2000). The PCA is used to investigate the domain pattern of the air ion mobility and their boundaries between different groups of ions. The principal components usually depend on the units used in the measurements and the ranges of values assumed by the original variables. Therefore, the data are standardized before PCA application. In the present case, the fractions of ion mobility spectra were treated with a nonlinear transformation by logarithmic scaling. It transforms the asymmetric frequency distributions of fractions concentration close to the normal, and the scaling did not significantly affect the classification of air ions (Horrak et al. 2000). Air ion fraction, equivalent diameter ranges for different classes of ions are given in Table 1, where N and P are the symbols of fraction for negative and positive polarity. The fractions are made according to the classes of air ions spectrum (Horrak et al. 2000; Gautam et al. 2017). The results from the PCA are shown in Sect. 4.4, where the top panels depict the negative and positive ions on non-event days (222) and the bottom panels for the event days (28). The components which have the highest percentage of contribution to the ion mobility distribution have been plotted in each panel. The total principal components that can be potentially extracted are limited to the number of variables, i.e., the number of fractions (20) in our case.

Table 1 Air ion fraction, equivalent diameter ranges for different classification of ions. N and P are the symbols of fraction for negative and positive polarity

Fraction	Mobility ($cm^2\ V^{-1}\ s^{-1}$)	Diameter (nm)
Small cluster ions		
N_1/P_1	2.37–3.16	0.36–0.62
N_2/P_2	1.78–2.37	0.62–0.81
N_3/P_3	1.33–1.78	0.81–1.03
Big cluster ions		
N_4/P_4	1–1.33	1.03–1.27
N_5/P_5	0.75–7	1.27–1.45
N_6/P_6	0.56–0.75	1.49–1.73
N_7/P_7	0.422–0.56	1.73–1.99
Intermediate ions		
N_8/P_8	0.316–0.422	1.99–2.34
N_9/P_9	0.237–0.316	2.34–2.76
N_{10}/P_{10}	0.178–0.237	2.76–3.35
N_{11}/P_{11}	0.135–0.178	3.35–3.90
N_{12}/P_{12}	0.1–0.133	3.90–4.60
N_{13}/P_{13}	0.074–0.1	4.60–7.39
N_{14}/P_{14}	0.0316–0.075	7.39–10.10
Light large ions		
N_{15}/P_{15}	0.0178–0.0316	10.10–13.80
N_{16}/P_{16}	0.01–0.0178	13.80–21.9
N_{17}/P_{17}	0.0042–0.01	21.9–29.5
Heavy large ions		
N_{18}/P_{18}	0.00237–0.0042	29.5–36.4
N_{19}/P_{19}	0.00178–0.00237	34.53–40.9
N_{20}/P_{20}	0.00133–0.00178	40.9–47.1

3 Results and Discussion

The formation of new particles in nucleation events occurs in a burst of intermediate ions (Horrak et al. 1998) and generally starts from cluster ions to large ions (Dal Maso et al. 2005; Hirsikko et al. 2005). Such events are easily noted with during the visual inspection of the diurnal variation of the number size distribution of positive and negative ions (Siingh et al. 2018). The days having such patches/shapes are called event days. In the absence of events, the spectrum appears almost uniform, and the day is termed as a non-event day. Types of new particle formation are generally categorized by the shape of the diameter spectrum in which the pattern of growth appears (Dal Maso et al. 2005). Based on these studies, Siingh et al. (2018) have recently presented class I—truncated banana shape, class II-patchy type, class III-inverted cup, and undefined (class IV) —not definite shape for event day and best example for non-event day. Randomly spectrums are rechecked so that chances of events being left out are relatively reduced. However, some deviations from these trends do exist in some cases. It is difficult to quantify the variations vary from event to event. The growth rate (GR) of ions was calculated using the mode fitting method (Hirsikko et al. 2005; Siingh et al. 2013b).

3.1 Diurnal Variation of Air Ions

For ready reference, an example of diurnal variation of the number size distributions of ions of both polarities on an event day (22 May 2012) is shown in Fig. 1. The shape of the spectrum may slightly change from season to season due to a minor shift in time and magnitude of the maxima caused by variations in solar radiation and local meteorological conditions. The third panel shows the diurnal variations of total ion concentrations of both polarities in the mobility range of 3.14–0.00133 $cm^2\ V^{-1}\ s^{-1}$ (0.36–47.1 nm diameter). The particle growth started from the size range 4–6 nm at 0900 h. The NPF event neither showed any simultaneous burst of small ions nor any persistent growth of ions of < 4–6 nm diameter, typical features of banana-type NPF events (Siingh et al. 2018). The particle growth rate during the event was found to be 6.58 ± 1.7 nm h^{-1} (6.67 ± 1.98 nm h^{-1}) for negative ions (positive ions) in the range of 5.4–47.1 nm. The truncated banana-type NPF events have different properties for different polarities. For example, the mean growth rate

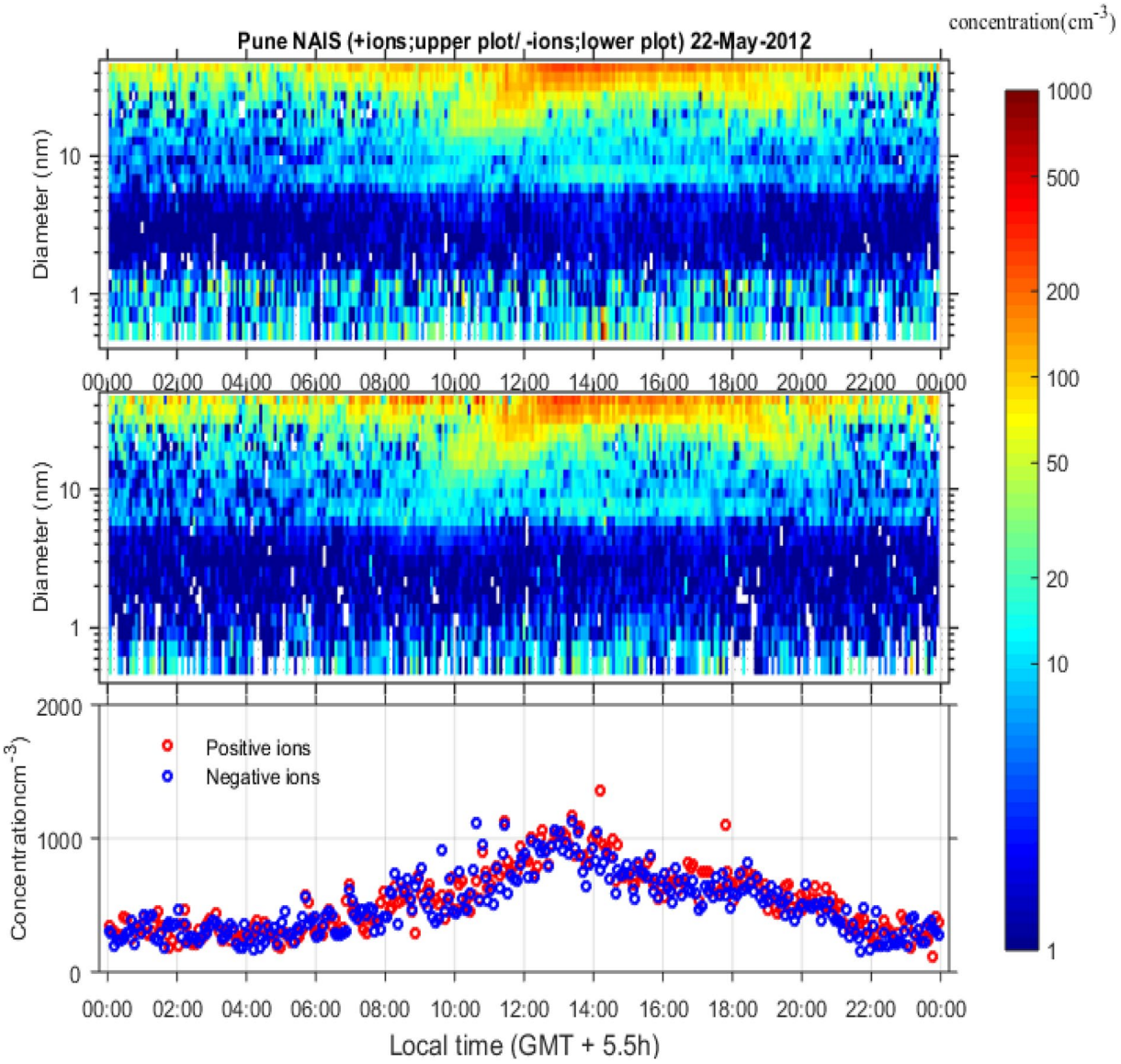

Fig. 1 An event day example for the diurnal variation of the number size distributions of positive and negative ions on 22 May 2012 at Pune, India. Lower panel shows diurnal variations of total ion concentrations of both polarities in the mobility range of 3.14–0.00133 $cm^2\ V^{-1}\ s^{-1}$ (0.36–47.1 nm diameter)

of positive ions ranged 7.23 ± 2.87 nm h^{-1} and for negative ions 8.5 ± 3.24 nm h^{-1} for ions in size range of 3.9–25.3 nm (fraction 12–16) (Table 1). Ions in the size range from 25.3 to 47.8 nm (fraction 17–20) (Table 1), the growth rates are 5.23 ± 2.03 nm h^{-1} for positive ions and 6.15 ± 3.1 nm h^{-1} for negative ions. Formation of new particles may start as molecular clusters at the top of the hills surrounding the institute, where solar radiation hits the before the valley. These newly formed particles along with other aerosol particles, and trace gases may be transported by katabatic winds (Kamra et al. 2015b; Gautam et al. 2017; Siingh et al. 2018). These molecular clusters formed at the top of the hill may grow to the nucleation mode particle (intermediate ions) during their transportation under nocturnal inversion along the hill-slope to the observation site (Kamra et al. 2015b). It takes about 2–3 h for the particles of 2–3 nm size to grow (by condensation and self-coagulation) into the nucleation mode size range of 9.7–15 nm (Kamra et al. 2015b). The absence of ions growth in the cluster size ranges can be inferred from the shift of a spectral peak. This result is consistent with the nanometer particle growth rates observed at clean continental sites (Weber et al. 1997; Mäkelä et al. 2000).

Figure 2 shows the diurnal variation (hourly mean concentration) of positive/negative ions in different mobility range for event and non-event days. Results are presented in

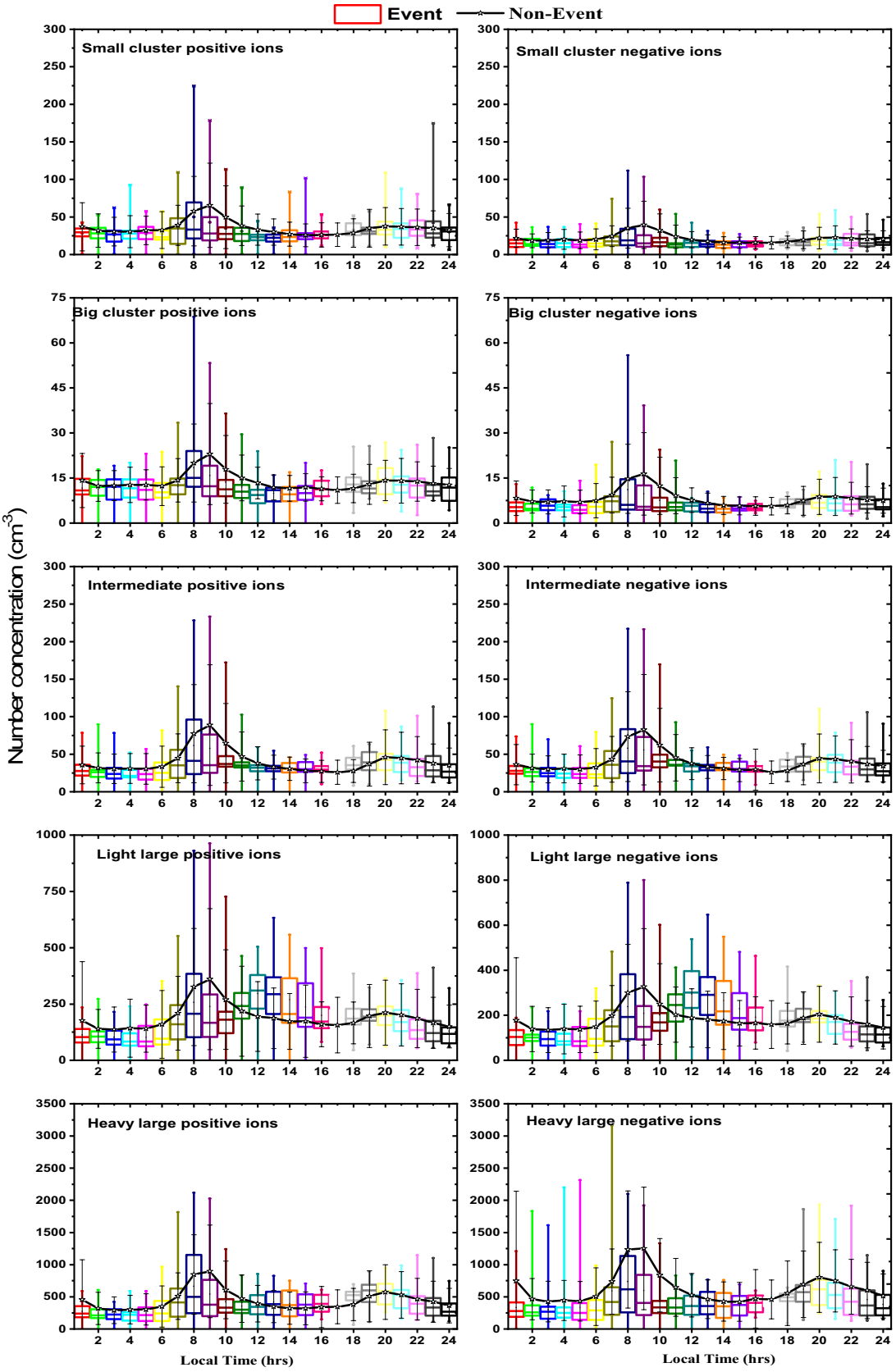

Fig. 2 Whiskers diagram of the diurnal variation (hourly mean concentration) of different categories ion distribution during event days (28 day mean) and non-event days (222 days mean; solid line), Pune, India

whisker plots for event days because NPF occurred mainly during post sunrise hours with a few events in mid of the day. Further, schematic growth of ions can be discerned up to 4 hours from the time of NPF occurrence on light large and heavy large ions which are substantially higher than annual values. The diurnal maximum distribution was observed at 0800 h and minimum around noon time at 1200–1400 h. The ion concentration gradually increased from noon time to 1900–2100 h. The upper quartile was higher during the morning hours for both the polarities, which shifted the mean above the median. The distributions were more comprehensive in the morning hours whereas the maximum occurred in the post evening hours. For non-event days, the diurnal pattern of all categories of ions was almost similar with differing amplitude throughout the year. Hence variation is shown by the mean curve. On non-event days, the concentration maximum in diurnal variation occurred at 0900 h and the minimum was observed during long period of 1300–1800 h. The mean concentrations also showed a little increase in the evening hours. The diurnal patterns of both the polarities were nearly similar but differed in their concentrations. The outliers of the positive and negative ions during morning hours on event days mostly coincided with period of NPF. The increasing concentration of ions during morning hours due to the particle formation on NPF days shifts the primary maximum of ions to earlier hour than non-event days. The big cluster ions concentrations had similar diurnal pattern as small cluster ions but had lower concentrations during the both event and non-event days. Negative ion concentrations in big clusters on event days had relatively more outliers than small cluster ions. Whisker diagram clearly shows the difference between negative ions outliers and positive ions outliers in different ranges of ions and their diurnal variations. The average diurnal variation of small ion concentration during 1993–1994 at Tahkuse Observatory, Estonia, showed the maximum at 0600–0700 h and the minimum at 1800 h for both negative and positive polarity (Horrak et al. 2000; Horrak 2001). Dhanorkar and Kamra (1993a) also reported the average diurnal variation of small ions concentration at Pune with the maximum concentration at 0500–0600 h and the minimum in the afternoon. The time of peak concentrations generally depend on the height of the measurement, surrounding terrain and evolution of boundary layer, etc. (Pal et al. 2014).

The size distribution of aerosol is strongly affected by photochemical nucleation bursts occurring under favorable meteorological conditions (for example, higher temperature/solar radiation, lower relative humidity with stable surface wind speed and direction) (Horrak et al. 1998; Siingh et al. 2013b, 2018). The diurnal variation of intermediate ions was similar to that of small ions (small cluster and big cluster ions) at this site. Positive and negative intermediate ions followed almost the same diurnal trend and their concentrations were approximately the same on both event and non-event days. However, during the morning hours (0700–0800 h) of NPF events, the ion concentration of both polarities showed a higher magnitude than that of non-event days. The NPF initiates from 4 to 6 nm diameter range (Kamra et al. 2015b; Siingh et al. 2018) and then ions gradually grow towards a higher diameter. On non-event days, the diurnal pattern of light large ions was similar to that of small and intermediate ions. However, on event days, the ion concentrations of both the polarities were higher than on non-event days from 1000 to 1600 h. During this period, the lower quartile was higher in the first 3 hours (1100–1300 h) and the upper quartile was more in the later 3 hours. The decreasing rate of ions concentration is more gradual for positive ions than negative ions. The rapid decrease of negative ions may be due to its property of faster coagulation or recombination with prevailing aerosol or opposite polarities. The latter scenario initiated from the big cluster, gradually appeared on intermediate and large ions. The positive ions outliers are higher than negative ions during event days.

Heavy large ions of both polarities had a similar trend during morning hours on non-event days. During 1200 to 1600 h, ion distribution is symmetrical irrespective of their charge, where the upper and lower quartiles were equally distributed. For negative ions, the outliers are exceptionally higher throughout the night. The event-day concentrations were slightly higher than that of non-event-days. The total ions concentration during event days is relatively higher, sometimes double than the non-event days. Another factor affecting the total concentration is the occurrence of a period of enhanced concentrations of ions and aerosols (PECIA) 2–3 h before NPF. In the PECIA periods, ions of ≤ 8 nm grow faster and attain mode diameter, which dramatically reduces the condensation sinks and may be conducive for particle formation (Kamra et al. 2015b). Though PECIA was not always associated with NPF, it frequently occurs in the early morning hours and rarely in the evening hours (Kamra et al. 2015a, b). It sustains for minutes to hour by increasing larger ions concentration to a certain extent, which is reflected in the total concentration on event days.

The distribution of different classes of air ions on event and non-event days demonstrated the differences at a diurnal scale. The significant changes between the daily mean of non-event days (222 days) and whisker diagram of event-days are due to the occurrences of new particle formation and its associated interaction with prevailing aerosol through recombination and coagulation processes (Kamra et al. 2015b). The primary maximum observed between 0800 and 0900 h is related to the breakdown of nocturnal inversion and convection of airmass from the earth surface upward to the measurement level. The changes in the mobility spectrum of small ions are due to the changes in the chemical composition and concentration of some trace gases or vapors

in the air probably generated by photochemical reactions. There was no substantial difference found between large ions of negative and positive polarity. Bursts or event of intermediate ions were not observed, whereas Siingh et al. (2013b) have reported a few numbers of events during the cloudy environment over this site. The present observations of similar behavior of small, intermediate and large ions to nanometer aerosol particles support the earlier results reported by Horrak et al. (2000, 2003). The higher concentrations of the small and intermediate ions of positive polarity on event days than that of negative polarity may be due to the electrode effect manifested close to the ground on the hill–slope and the local topography of site (Porstendorfer 1994). In addition, higher positive ion may also be related to the availability of nucleating/growing vapors since certain vapors may favor the formation and growth of ions in single polarity (Siingh et al. 2018). The katabatic winds flowing down along the hill-slope surrounding the site in the morning hours may transport and keep depositing an excess positive ion and positively charged particles along with the radioactive emanations and trace gases in the valley (Kamra et al. 2015b). Dhanorkar and Kamra (1993b) and Kamsali et al. (2003) reported enhanced concentration of ^{222}Rn and its progeny in the morning hours in coincidence with the peaks in electrical conductivity. Figure 3 clearly showed the presence of additional ionization in the morning hours. In contrast to the small and intermediate ions, no significant differences between the negative and positive light large and heavy large ions concentrations were observed (Fig. 2).

Recently, Gautam et al. (2017) analyzed NAIS observation from the same site and reported a higher percentage of relative standard deviation (RSD) for negative ions and a lower rate for positive ions. Moreover, this deviation was also different for day and night time. In general, the RSD may vary depending on various atmospheric factors such as the origin of air masses, presence of low-volatile vapors, aerosol precursor vapors, pre-existing aerosol concentrations and meteorological parameters. In addition, chemical composition of the cluster ions and solar radiation also control the nucleation and growth rates (Boy and Kulmala 2002; Bonn et al. 2009). The low condensational sink of vapors and characteristic nighttime temperature inversions and intensive mixing of boundary layer air at daytime may provide favorable conditions for nucleation (Kulmala et al. 1998; Clement et al. 2001).

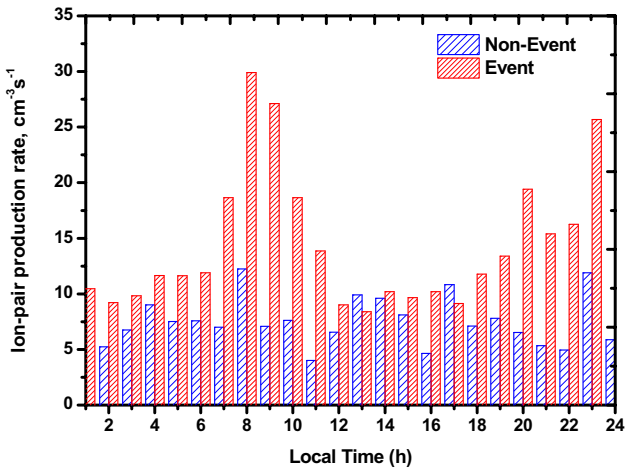

Fig. 3 Mean diurnal variation of ion-pair production rate calculated from small ions observations on event (28 days mean) and non-event days (222 days mean) for the year 2012

3.2 Ion-Pair Production Rate

The mean diurnal variation of ion-pair production rate (Fig. 3) for non-event days shows similar pattern as the cluster ion concentration with the mean of 6.5 ion pairs cm^{-3} s^{-1}. The ionization on event days (Fig. 3) gradually increased from morning hours and maximized at ~ 0800–0900 h. Thereafter sharply decreased and became almost equal to non-event days value during noon hours. From 1600 h onward, the ion-pair production rate for non-event days again started increasing trend with a secondary maximum ~ 2300 h. The timings of maxima roughly coincided with the breakdown of stability conditions of ABL. Also the timing of minimum roughly coincided with the time of maximum turbulence in the ABL during the afternoon. After the minimum, a gradual increase in ion concentration was associated with the night time steady boundary layer development. The mean ion-pair production rate on event days varied ~ 20 ion pairs cm^{-3} s^{-1}. The direct connections between the ionization rate and the cluster ions formation are reflected in their diurnal variation during NPF, with some dissimilarities associated with varying atmospheric conditions and dynamical processes. Chen et al. (2016a) showed that the ^{222}Rn concentration at near ground level does not respond immediately to mixing layer expansion or shrinkage. However, Chen et al. (2016b) reported that the cluster ion concentrations are related to the ionization process, to photochemical processes and availability of nucleating vapors influenced by solar intensity and atmospheric conditions. The large number of events observed during summer days (pre-monsoon) supports the above hypothesis. During summer, increased solar radiation enhances the photoionization, enhancing ion cluster formation at the top of the surrounding hills. Later, solar radiation hit the surface near the observatory leading to surface heating, turbulence and mixing layer development. All these may assist the increased formation of vapors which is helpful in the nucleation and growth of cluster ions.

Figure 4a showed variations of computed daily ion-pair production rate (Q) (Eq. 2) from the measurements of ion

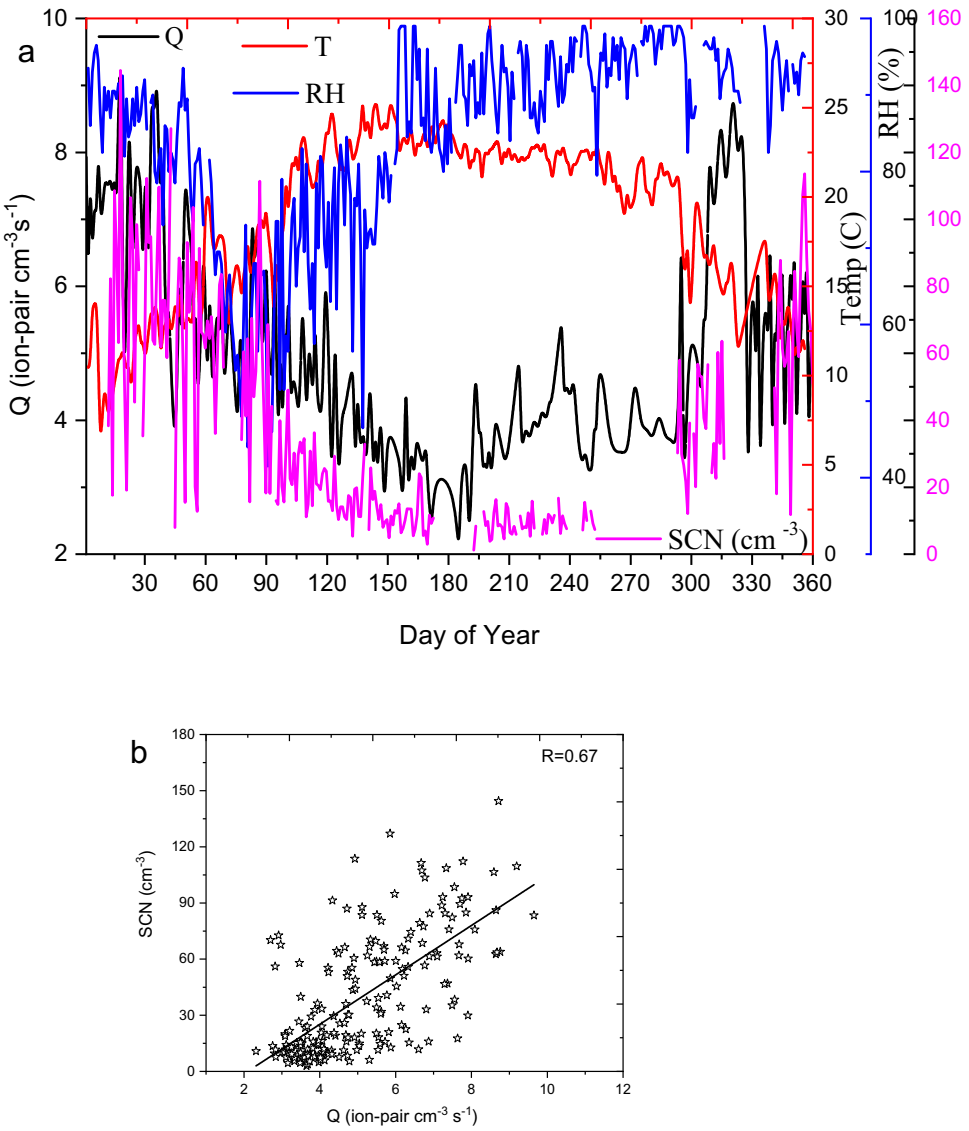

Fig. 4 **a** Variation of daily ion-pair production rate (Q) derived from ^{222}Rn and its progenies (0800 h) and temperature ($T_{min.}$), relative humidity (RH max.) ($T_{min.}$ and RH max are the mean of 0600–0700 h of the day) and corresponding small cluster negative ions (SCN) concentration (0800 h) of the day (**a**); correlation coefficient between small cluster ions and ion-pair production rate (**b**)

concentrations and radioactive ^{222}Rn and its progeny. It should be noted that the breaking of nocturnal inversion layer and its influence on small ion concentrations usually take ~ 2 h (Pal et al. 2014). The same is applied for the consideration of temperature (T_{min}), relative humidity (RH max) at 0600–0700 h and ions concentration at 0800 h. Horrak et al. (2000) based on multiple regression analysis reported that RH and heavy large ion concentration are the main factors that affect the natural mean mobility of small ions (Horrak 2001). Solar radiation and hence temperature are the fundamental factors that affect small ion distribution (Kulmala et al. 1998). Daily variation of Q and small cluster ion concentration at 0800 h significantly follow each other, except during the monsoon season (JJAS). The minimum temperature (T_{min}) and maximum RH indicate the period at which thermal layer is stable, as the T_{min} value increases towards pre-monsoon (MAM), the breaking of the nocturnal stability become relatively stronger than other seasons. This result in to the strong dissipation of the Radon emitted from the soil and Q is gradually decreased (Chen et al. 2016a). The relation became complex during the monsoon season (JJAS), when the source and sink of the small ions behave differently. The rainwater blocks ^{222}Rn emission from the soil and larger aerosol ions are also removed from the atmosphere by wet scavenging. Hence, the small cluster ions became extremely low (< 20 cm-3) during morning hours. However, due to the capping effect, a sudden increase of Radon concentration may be observed occasionally during the initial periods of rainfall (Schumann et al. 1988; Victor et al. 2019). From post-monsoon (ON), the normal relation between temperature, Q, and small cluster ions was observed. Apart from the temperature and RH, the change in diurnal variation of wind speed also impacts the concentration of Radon, air ions/ aerosol particles and hence Q by advection. Figure 4b

clearly showed that small cluster ion was well correlated with ion production rate having a correlation coefficient of 0.67 with 95% significance level. The concentration of small clusters and ion-pair production rate showed similar behavior throughout the year. However, T_{min} and RH have nearly opposite trends. The ionizing radiation is primarily controlled by many atmospheric parameters such as boundary layer depth, air temperature, wind speed, solar radiation, soil characteristics, etc. In addition, the long transportation of air masses to the measurement site may bring extra Radon concentrations. Dal Maso et al. (2005) reported that low Radon ionizing capacities were found in association with NPF events which is in agreement with our ^{222}Rn observation and statistics on NPF events at Pune (Siingh et al. 2018).

3.3 Conductivity Relation with Ion Concentration

The present air ions observations are used to compute polar conductivity using the relation $\sigma = \mu\, n_{i/p}\, e$, where μ is mobility, n is small ions concentration and e electric charge 1.6×10^{-19} C. The variation of mobility and polar conductivity with respective ion concentrations on the event and non-event days are presented in Fig. 5. Positive ion concentration on event days showed two peaks with departure from non-event days corresponding to mobility 0.003 and 0.03 cm^2 V^{-1} s^{-1} whereas no many peaks could be seen for negative ions. The same was valid for conductivity. The sum of total conductivity on event days for all the mobility range is 3.313 f S m^{-1}. In which, small ion (mobility ranges 3.16–0.5 cm^2 V^{-1} s^{-1}) contributed 3.076 f S m^{-1} and large ions (mobility ranges 0.034–0.00133 cm^2 V^{-1} s^{-1}) accounted only 0.112 f S m^{-1}, that is 92.84% contribution of conductivity was by small ions and only 3.68% by large ions in the total conductivity. The remaining percentage was contributed by the intermediate ions (mobility ranges 0.5–0.034 cm^2 V^{-1} s^{-1}).

Similarly, for non-event days, small ions had more than 93.66% contribution and larger ions accounted only for 2.73% of total conductivity. The conductivity range observed at this site is approximately two folds lower than that of the rural atmosphere because of the more significant amount of small ion concentrations and less aerosol particles (Horrak et al. 2000). The increasing (decreasing) trend in conductivity by small ions (large ions) indicates the decreasing aerosol concentration before the NPF periods (Kamra et al. 2015b). The decrease in aerosol concentration leads to a reduction in the ion-aerosol attachment, which causes a change in the

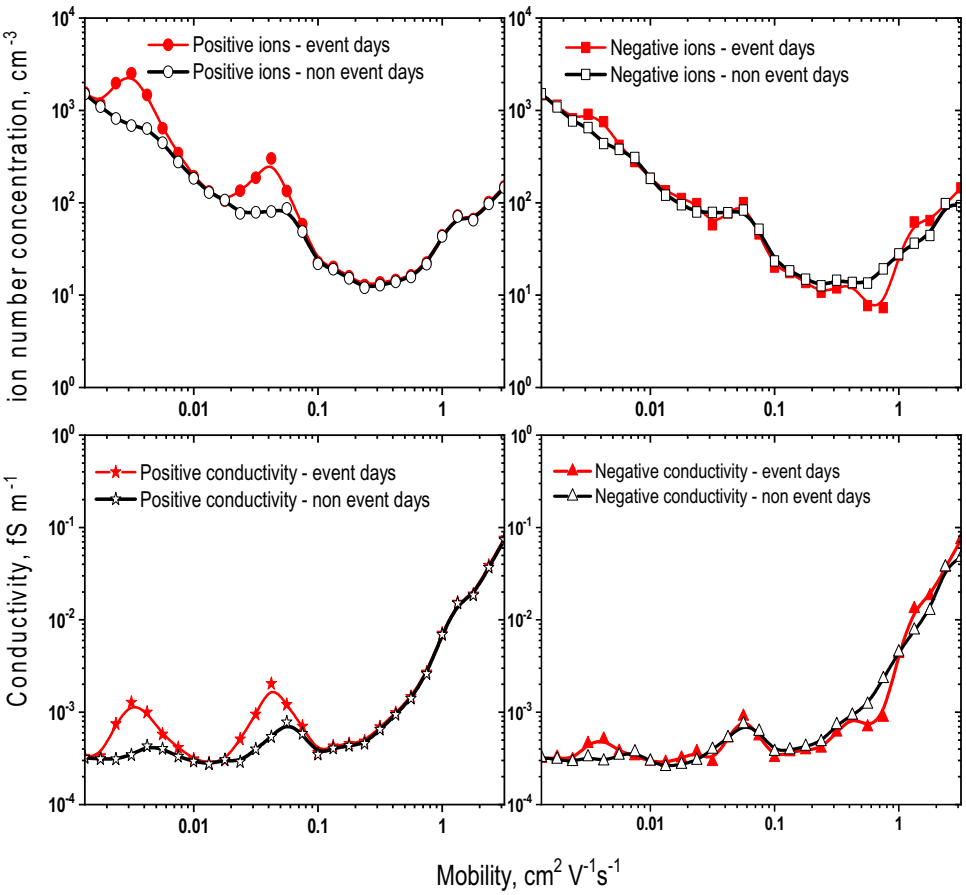

Fig. 5 Variation of mobility with ion number concentrations (both polarities) along with conductivity (both polarities) for event (28 days mean) and non-event (222 days mean) days

conductivity. The difference between positive and negative conductivity decreases with increasing ions size/diameter.

Earlier study by Dhanorkar and Kamra (1993b) reported that small ions contributed more than 95% on most of the days and intermediate ions contribution was little higher than large ions. Further, they also found that this ratio varied from season to season. It is to be noted that ionization production by Radon concentration highly depends on the season (Kamsali et al. 2003). A similar study from the middle latitude station suggested that the small ions contributed 96.3% (5.95 ± 2.11), intermediate ions for 2.2%, and large ions for 1.5% of total conductivity (Horrak et al. 2000). The reported measurement site was mostly masked by the wintering snowfall and its aggregation. Another observation in a pristine condition at Antarctica reported that the conductivity is only due to small ions and varied with the annual mean of 7.5 ± 1.5 f S m^{-1} (Siingh et al. 2013c). They further reported that the value was consistent with the atmospheric electric current and field measurements.

Variations in the ion production rate are primarily related to the atmospheric boundary layer (ABL) development, soil conditions and origin of air masses (Siingh et al. 2018; Victor et al., 2019). ^{222}Rn concentration is strongly related to the vertical stability of the ABL (Kataoka et al. 1998). Recently, Victor et al. (2019) discussed that ^{222}Rn concentration and ionization decreased with the increase of upward wind velocity in the ABL and moisture of the soil for different seasons. The dynamics of ABL plays crucial role in the exchange of energy, moisture, momentum and pollutants from surface to upper layers (Lee et al. 2015). Nilsson et al (2001a, b) discussed in detail the effect of air masses, synoptic weather and boundary layer evolution on aerosol formation. The generations of intermediate ions after sunrise with a delay of 2–3 h (Fig. 2) coincide with the rapid development of the boundary layer. ^{222}Rn and its progenies may be the major source of surface ionization of air molecules, however, the lack of association between the mobility ranges are because of the modification of atmospheric air ion properties exerted by different dynamical and chemical processes during the evolution of changes in the atmosphere. The concentration of small ions was found to be dependent on aerosol concentration and hence only heavy large ion concentration due to ion-aerosol attachment (Hoppel 1985), the stability of air close to the ground, and the state of the soil (in terms of radioactive molecule concentration) (Chen et al. 2016b; Victor et al, 2019). The difference in the concentration of positive and negative ions in size range < 1.6 nm (small ions) can be explained by the two factors, (1) during morning hours, deposition of the ions and particles from the hilltop surface to the valley by katabatic winds and (2) due to the electrode effect. Positive ions and particles tend to settle down on the surface of the Earth. These result in the excess positive ions of small size diameter at our measurement site.

3.4 Principal Component and Factor Analysis

Figure 6 shows the factors of air ion mobility spectra for both polarities (positive and negative) of air ions during event (28 days mean) and non-event (222 days mean). Measurements used in the verification of the classification of ions are required to have fractions that match close to the mobility classes. The first five principal components substantially explained about 98% (99%) and 94% (96%) of total variance for positive (negative) ions on non-event and event days, respectively. The first principal component explained about 87% (86%) and 58% (65%) of total variance for positive (negative) ions on non-event and event days, respectively. The contribution of rest components and their location of peak-fraction are shown in Fig. 6. The noticeable difference is the contribution of the second component which is only 5% (5%) and 22% (18%) for positive (negative) ions on non-event and event days, respectively. The peak contributions for both types of ions are from fraction 13 (diameter 4.60–7.39 nm) and fraction 16 (diameter 13.80–21.9 nm) non-event and event days. The difference in contribution and structure of different components at various fractions on event days from non-event days arrived due to differential response of growth of ions in different categories or size range and shapes.

In general, the atmospheric nucleation initiates once air ions reached the critical cluster size of 1.5 ± 0.3 nm (Kulmala et al. 2013), from that place the growth of a cluster is energetically favored (Vehkamaki 2006). Further, the charged clusters on event days grow faster than the same size neutral particles (Kamra et al. 2015a). Kamra et al. (2015b) reported the mean growth rates of 3.9–25.3 nm (fraction 12–17) positive (negative) ions to be 49–142% (49–126%) and the growth percentage was more significant for those having size in the range 25.3–47.8 nm (fraction 17–20). Gautam et al. (2017) reported that different polarities of ions have different growth rate for other classes of air ions. Another factor affecting the variance in contribution of various components is the production rate of charged particles by the attachment of ions with aerosol particles, which are higher in size range of 3.85–7.4 nm diameter (fraction 11–13) as compared to the other sizes ranges. Additionally, ion-ion recombination rate also increases with the enhanced concentration of ions and particles. Meteorological parameters may also change the structure of ion concentration through changes in residence time, diffusion, and removal from the measurement location (Jaenicke 1984; Hoppel et al. 1990).

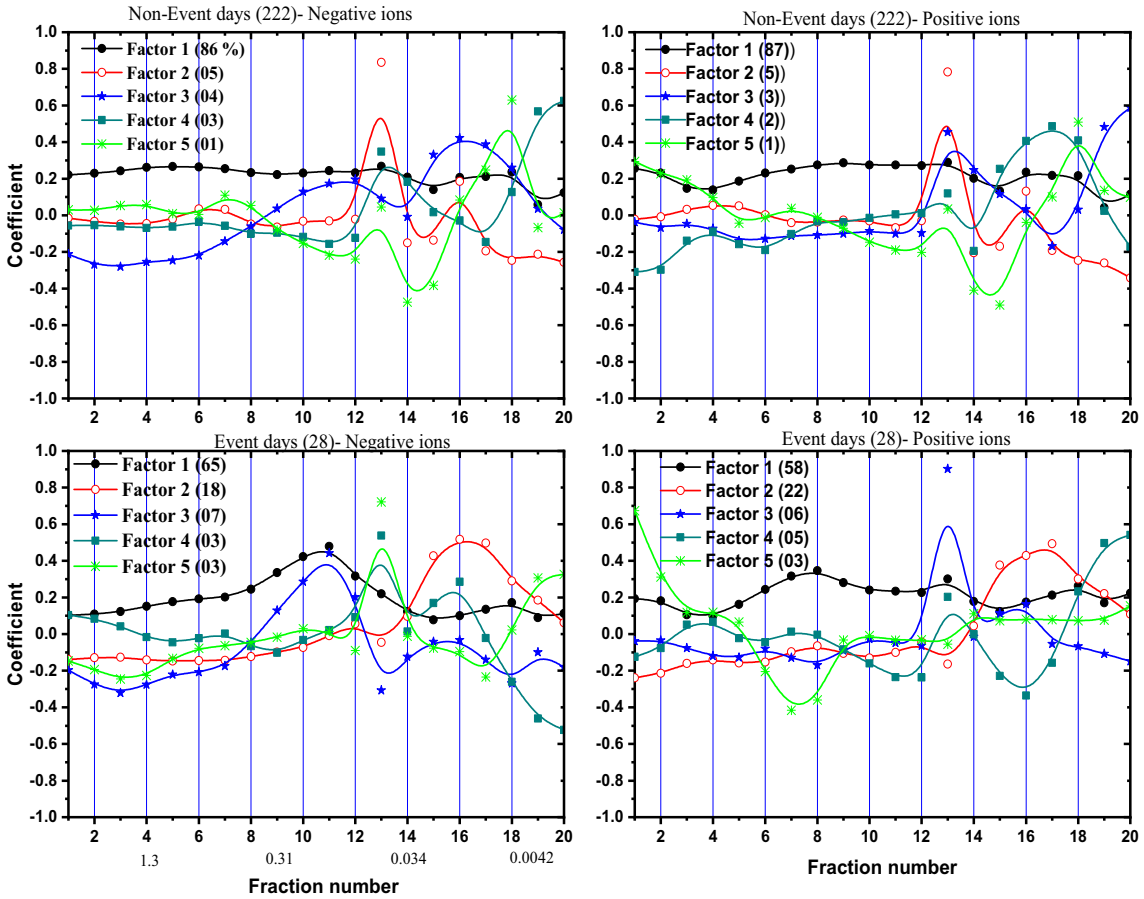

Fig. 6 Factors of air ion mobility spectra for positive and negative ions for event (28 days mean) and non-event (222 days mean). The mobility and diameter boundaries of fractions are given in Table 1. Percentage of contribution of the factor to that of total variation is given in the bracket of each panel

Fractional concentration of mobility spectrum of air ions may also be interpreted as a set of closely correlated variables (Table 1). Correlation coefficient in percent between atmospheric air ion mobility fractions during non-event days for the year 2012 for both the polarities of ions are given in Table 2**.** The formal correlation is attributed to (1) physical and chemical processes embracing a group of fractions (i.e., positive correlation) or acting between different groups of fractions (i.e., negative correlation) and (2) an unavoidable smoothing of a spectrum due to the finite resolution of NAIS. Fractions 1 to 12 (diameter 0.3–4.6 nm) consistently show highly significant positive correlation (> 95%). For fraction 13 and 14, the linearity drastically decreased to 44% concerning fraction 1 and from fractions 15 to 20 (diameter 10.10–47.1 nm) the average correlation is > 90%. This fractional mobility is considered to be the boundary of the above fractions (> 0.076 $cm^2\ V^{-1}\ S^{-1}$) on the other hand, the physical/ chemical processes of intermediate ions were highly pronounced for this fraction (at F13 and F14, 4.6 nm). This finding is in good agreement with the earlier measurements made at this site with the conventional Gerdien condenser technique (Dhanorkar and Kamra 1991). They reported the maxima at about 0.076 $cm^2\ V^{-1}\ s^{-1}$ (diameter 4.6 nm) for intermediate ions, which have the highest variability in the mobility spectrum. Usually, during their generation by photochemical nucleation, the peak particle size shifts toward the larger sizes in the spectrum (Misaki 1964; Kojima 1984). The mode diameter fraction (N13 and N14) of intermediate ions show good correlation (73% and 60%) with the fraction N16, which is the mode diameter of light large ions (diameter,13.80–21.9 nm). For positive ions, the scenario is quite different because they are likely to encounter fewer molecules in its path than negative ions. Hence, they have relatively lower growth rate than the negative ions. Fraction 1–16 had correlation > 90%. The least correlation (~ 88%) was between fraction 18 and fractions 4–5. A negative correlation was not observed on non-event days.

Table 3 showed the correlation between mobility fractions for positive and negative ions on the event days. For negative ions, the correlation for fractions 1 to 12 gradually decreased

Table 2 Correlation coefficients (in percent) between air ion- mobility fractions for negative and positive ions during non-event days (222) for the year 2012

Negative ions-non-event days (222)																				
FN	N1	N2	N3	N4	N5	N6	N7	N8	N9	N10	N11	N12	N13	N14	N15	N16	N17	N18	N19	N20
N1	100	99	99	99	99	99	98	98	97	96	95	95	60	44	91	87	87	90	92	94
N2	99	100	99	99	99	99	98	98	97	95	95	94	59	43	90	85	86	89	92	93
N3	99	99	100	99	99	99	98	98	97	95	95	94	58	42	90	86	87	90	93	94
N4	99	99	99	100	99	99	99	99	98	96	96	95	59	42	92	87	88	92	94	95
N5	99	99	99	99	100	99	99	99	98	97	96	95	60	44	92	88	88	91	94	95
N6	99	99	99	99	99	100	99	99	98	97	96	96	64	48	92	89	88	91	93	94
N7	98	98	98	99	99	99	100	99	98	97	97	96	64	48	93	91	90	93	95	95
N8	98	98	98	99	99	99	99	100	99	98	98	97	58	42	95	91	92	94	95	96
N9	97	97	97	98	98	98	98	99	100	99	99	98	57	40	96	92	94	94	94	95
N10	96	95	95	96	97	97	97	98	99	100	99	99	58	41	98	94	95	93	93	94
N11	95	95	95	96	96	96	97	98	99	99	100	99	57	40	98	94	95	93	92	93
N12	95	94	94	95	95	96	96	97	98	99	99	100	58	41	98	94	95	92	92	93
N13	60	59	58	59	60	64	64	58	57	58	57	58	100	97	53	73	46	48	55	52
N14	44	43	42	42	44	48	48	42	40	41	40	41	97	100	36	60	29	31	39	35
N15	91	90	90	92	92	92	93	95	96	98	98	98	53	36	100	95	98	93	90	91
N16	87	85	86	87	88	89	91	91	92	94	94	94	73	60	95	100	93	88	87	87
N17	87	86	87	88	88	88	90	92	94	95	95	95	46	29	98	93	100	96	91	92
N18	90	89	90	92	91	91	93	94	94	93	93	92	48	31	93	88	96	100	98	98
N19	92	92	93	94	94	93	95	95	94	93	92	92	55	39	90	87	91	98	100	99
N20	94	93	94	95	95	94	95	96	95	94	93	93	52	35	91	87	92	98	99	100
Positive ions-non-event days (222)																				
FN	N1	N2	N3	N4	N5	N6	N7	N8	N9	N10	N11	N12	N13	N14	N15	N16	N17	N18	N19	N20
N1	100	99	97	97	97	98	98	98	98	97	97	97	97	97	94	92	91	90	93	95
N2	99	100	99	98	98	99	98	98	98	98	97	97	98	97	94	92	90	89	94	95
N3	97	99	100	99	98	98	98	97	97	97	96	96	97	96	93	91	89	89	93	94
N4	97	98	99	100	99	98	98	98	98	98	97	97	97	96	94	93	90	88	92	93
N5	97	98	98	99	100	99	98	98	99	98	98	98	98	97	95	94	90	88	91	92
N6	98	99	98	98	99	100	99	99	99	99	99	99	99	98	96	95	92	89	93	94
N7	98	98	98	98	98	99	100	99	99	99	99	99	99	98	97	96	93	92	94	95
N8	98	98	97	98	98	99	99	100	99	99	99	99	99	99	98	97	94	93	95	95
N9	98	98	97	98	99	99	99	99	100	99	99	99	99	99	98	97	94	92	94	95
N10	97	98	97	98	98	99	99	99	99	100	99	99	99	99	98	97	94	92	94	94
N11	97	97	96	97	98	99	99	99	99	99	100	99	99	99	98	97	95	92	94	94
N12	97	97	96	97	98	99	99	99	99	99	99	100	99	99	98	97	95	92	94	94
N13	97	98	97	97	98	99	99	99	99	99	99	99	100	99	98	97	94	93	95	95
N14	97	97	96	96	97	98	98	99	99	99	99	99	99	100	97	96	93	92	95	95
N15	94	94	93	94	95	96	97	98	98	98	98	98	98	97	100	99	97	94	94	93
N16	92	92	91	93	94	95	96	97	97	97	97	97	97	96	99	100	98	95	94	93
N17	91	90	89	90	90	92	93	94	94	94	95	95	94	93	97	98	100	97	95	94
N18	90	89	89	88	88	89	92	93	92	92	92	92	93	92	94	95	97	100	98	97
N19	93	94	93	92	91	93	94	95	94	94	94	94	95	95	94	94	95	98	100	99
N20	95	95	94	93	92	94	95	95	95	94	94	94	95	95	93	93	94	97	99	100

FN fraction number

Table 3 Correlation coefficients (in percent) between air ion-mobility fractions for negative and positive ions during event days (28) for the year 2012

Negative ions- event days (28)																				
FN	N1	N2	N3	N4	N5	N6	N7	N8	N9	N10	N11	N12	N13	N14	N15	N16	N17	N18	N19	N20
N1	100	94	88	90	89	90	89	82	75	72	67	62	43	34	− 7	− 15	16	20	67	75
N2	94	100	97	95	92	92	90	84	78	75	70	65	42	31	− 2	− 11	13	17	72	81
N3	88	97	100	97	92	91	88	84	80	77	72	68	37	25	0	− 8	8	11	75	82
N4	90	95	97	100	98	96	93	90	86	83	79	74	37	24	0	− 9	6	9	78	87
N5	89	92	92	98	100	98	96	94	90	87	83	77	42	30	0	− 9	12	15	79	89
N6	90	92	91	96	98	100	98	96	92	89	85	79	49	37	0	− 7	19	23	79	89
N7	89	90	88	93	96	98	100	97	92	89	84	78	51	39	1	− 7	22	25	74	84
N8	82	84	84	90	94	96	97	100	97	93	89	83	47	34	4	− 3	18	21	77	84
N9	75	78	80	86	90	92	92	97	100	97	93	87	45	31	10	4	17	19	76	81
N10	72	75	77	83	87	89	89	93	97	100	98	93	48	34	18	11	20	21	69	74
N11	67	70	72	79	83	85	84	89	93	98	100	98	44	30	31	23	16	15	60	67
N12	62	65	68	74	77	79	78	83	87	93	98	100	38	23	46	38	11	7	53	61
N13	43	42	37	37	42	49	51	47	45	48	44	38	100	98	7	5	93	93	37	39
N14	34	31	25	24	30	37	39	34	31	34	30	23	98	100	2	2	97	98	29	29
N15	− 7	− 2	0	0	0	0	1	4	10	18	31	46	7	2	100	98	6	− 7	− 13	− 6
N16	− 15	− 11	− 8	− 9	− 9	− 7	− 7	− 3	4	11	23	38	5	2	98	100	9	− 4	− 15	− 10
N17	16	13	8	6	12	19	22	18	17	20	16	11	93	97	6	9	100	98	16	15
N18	20	17	11	9	15	23	25	21	19	21	15	7	93	98	− 7	− 4	98	100	22	19
N19	67	72	75	78	79	79	74	77	76	69	60	53	37	29	− 13	− 15	16	22	100	93
N20	75	81	82	87	89	89	84	84	81	74	67	61	39	29	− 6	− 10	15	19	93	100
Positive ions-event days (28)																				
FN	N1	N2	N3	N4	N5	N6	N7	N8	N9	N10	N11	N12	N13	N14	N15	N16	N17	N18	N19	N20
N1	100	90	71	70	78	72	69	71	75	73	69	67	30	21	8	− 1	10	13	20	37
N2	90	100	90	84	91	88	83	83	88	86	82	80	39	28	8	− 1	16	18	27	47
N3	71	90	100	95	88	83	78	75	77	73	69	68	31	21	− 10	− 18	9	13	22	43
N4	70	84	95	100	92	82	78	75	77	73	69	68	22	12	− 9	− 18	0	4	14	36
N5	78	91	88	92	100	94	90	89	93	91	88	85	28	17	8	0	5	6	17	40
N6	72	88	83	82	94	100	97	94	96	93	90	88	40	29	20	12	20	19	29	51
N7	69	83	78	78	90	97	100	98	95	90	88	89	39	28	30	22	20	18	29	51
N8	71	83	75	75	89	94	98	100	97	91	91	92	34	22	35	27	15	12	24	47
N9	75	88	77	77	93	96	95	97	100	97	95	94	36	24	31	23	15	13	25	47
N10	73	86	73	73	91	93	90	91	97	100	98	94	39	27	27	19	18	16	27	47
N11	69	82	69	69	88	90	88	91	95	98	100	97	32	21	35	26	13	10	20	39
N12	67	80	68	68	85	88	89	92	94	94	97	100	28	16	46	37	9	5	15	35
N13	30	39	31	22	28	40	39	34	36	39	32	28	100	99	3	7	96	97	98	96
N14	21	28	21	12	17	29	28	22	24	27	21	16	99	100	0	4	98	99	99	93
N15	8	8	− 10	− 9	8	20	30	35	31	27	35	46	3	0	100	98	7	− 5	0	5
N16	− 1	− 1	− 18	− 18	0	12	22	27	23	19	26	37	7	4	98	100	14	1	5	9
N17	10	16	9	0	5	20	20	15	15	18	13	9	96	98	7	14	100	98	98	91
N18	13	18	13	4	6	19	18	12	13	16	10	5	97	99	− 5	1	98	100	99	91
N19	20	27	22	14	17	29	29	24	25	27	20	15	98	99	0	5	98	99	100	95
N20	37	47	43	36	40	51	51	47	47	47	39	35	96	93	5	9	91	91	95	100

FN fraction number

but remained higher than 62%, whereas it decreased from 43% to 15% for fractions from 13 to 16 (4.60–21.9 nm). In addition, the same negative correlation (−15%) was also observed between the fraction 19 and fraction 16. From fraction 17, the correlation became positive and improved to a high value. Earlier studies suggested that the formation and growth of the ions in the size range of 1.7–7.4 nm (fraction 7–13) during NPF events significantly increases the ion concentration. These excess ions along with existing small ions, get attached with natural particles and convert them into larger ions, which can be seen as positive correlations between N_6–N_{10} and N_{17}–N_{18} for negative ion. The high correlation (> 93%) between fractions N_{13}-N_{14} (diameter 4.60–10.10 nm) with fractions N_{17} and N_{18} (diameter, 21.9—36.4 nm) may be due to nucleation of new particle formation and subsequent growth of particles that comprise the light large ions (Horrak 2001). In the case of positive ions, the correlation varied from 99 to 18%. Fraction P_{13}–P_{14} had correlation > 93% with heavy larger ion segments (fractions P_{17}–P_{20}). Fraction P_1–P_5 showed very little or negative (8% to −18%) correlation with faction P_{15}–P_{16}. The disassociation mostly arises by the combined effect of temperature, moisture and background aerosol scavenging. The cluster ions were typically observed in the absence of solar radiation and hence in the absence of photosynthesis when the mixing layer is thin and possibly because they are produced in the smaller mixing volume and the further growth process by the prevailing vapors may be feeble.

The boundary of fractions may cause the lower positive correlation both on event and non-event days for the fractions 12–15 by different mobility ranges. Fraction 1 to 13 represents the individual NAIS channels and from fraction 14 to 20, the channels are grouped by more than 2. Positive ions on non-event days seem to have well-organized patterns to have well-organized variations so that the discrepancies were not appeared in this category. The higher correlation between the fractions of positive ions on non-event days suggested that the maximum sustainability of the positive ions in the atmosphere under recombination, aerosol attachment and coagulation process is relatively higher. In contrast, lower mobilities of negative ions may be due to lower lifetime and a higher rate of extension with prevailing higher size aerosol particles in the atmosphere.

During NPF events, the growth of the new particle mostly ceased when it reaches to the intermediate ion size (~7.4 nm, fraction 13) and their dissipation by recombination/combination process continues. This was commonly observed, which is also reported by Kamra et al. (2015a, b). Moreover, the coagulation of ions with aerosol particles is faster and more potent than for the same size neutral particles, since the larger electrostatic force contributes more to the attachment process. An increase in coagulation rate contributes for higher growth rate of particles during NPF events. The event would eventually decrease with increasing particle size (Yu and Turco 2001). In this study, we covered the entire year to maintain the significance of the statistical relation (Horrak 2001; Horrak et al. 2000), and hence the data consist of seasonal variability of air ions, including a comprehensive monsoon month (JJAS). Horrak (2001) explained the complexity in determining the boundaries between and within the separated classes on air ion and aerosol ion, especially in intermediate ions. They further stated that the levels of air ions have seasonal variability to a certain extent; hence mean value may be considered (Tammet 1995; Dhanorkar and Kamra 1991).

4 Conclusion

To understand the mobility, diurnal characteristics of atmospheric air ions of both polarities and their dependence on the meteorological parameters on event and non-event days, atmospheric ions and concentration of ^{222}Rn measurements carried out at Pune was analyzed. Annual mean diurnal variations of atmospheric air ions derived from 222 non-event days of observation show the bimodal distribution with the primary maximum in the morning at ~0800 h and the secondary maximum in the evening at ~1800 h, with the minimum concentration during 1200–1400 h local time. This diurnal cycle variation is observed for the air ions concentrations of the entire measured range of diameter 0.36–47.1 nm. Temperature and humidity affect ion distribution and boundary layer evolution and hence also Radon emission which is an important factor for ion production and its diurnal variation. Based on the present study following results are obtained:

1. From the diurnal variation, a link between the ionization rate and the cluster ions formation during new particle formation events was observed with small dissimilarities which may be attributed to the varying atmospheric conditions and dynamical processes. Further, it is also observed that larger size ions decreased before the onset of the particle formation, which increased conductivity. The boundary layer evolution and topography of the measurement site could explain maxima in the morning hours, minima in the afternoon and a secondary maximum of ion concentration in the evening hours.
2. A gradual and systematic growth of air ions is observed on event days, especially in the intermediate ions, which have a different diurnal pattern from the non-event days. It is interesting to note that air ions with large concentrations in different ranges are observed throughout the year, but most of the NPFs were observed during pre-monsoon months (MAM). This suggests that solar radiation along with temperature and humidity play sig-

nificant role in particle formation. Further, the concentration differences on event and non-event days are more prominent in larger ions segment (> 7.4 nm).

3. To investigate the dominant pattern of the air ion mobility spectrum, the principal component analysis (PCA) was used and showed that the first five components to a first approximation could represent about 98% of all the measured information in the mobility boundaries on non-event and event (NPF) days The first component explained ~ 86% (65%) of total variance on non-event (event) days and it is closely correlated with the respective ion classes. Linear regression analysis between the fractions demonstrates the boundaries of the classes of air ions. The mode diameter of intermediate ions at 4.6 nm (F13) prominently separate small ions from large ion's fractions.

Improved understanding of the evolution of atmospheric air ions on a diurnal scale helps to determine the role of boundary layer mixing and topography on NPF. However, along with air ions measurements, simultaneous aerosols, trace gases such as SO_2, NH_3, Iodine, VOC, ionization and metrological parameters made at different geographical locations over long periods is widely required to understand the possible generation mechanisms in different seasons completely.

Acknowledgements The Indian Institute of Tropical Meteorology, Pune is supported by the Ministry of Earth Sciences, Government of India. Authors thank the India Meteorological Department Observatory at Pune for providing the meteorological data. Author thanks to Dr A. K. Kamra for valuable suggestions. This work is supported under the collaboration program of IITM, Pune, and BHU, Varanasi, India. We are thankful to the anonymous reviewers for their constructive comments and valuable suggestions to improve the quality of the manuscript.

Author contributions JV and DS are responsible for inception and, execution of project and preparation of the draft of the manuscript. JV and DS analyzed the ion data and metrological data. JV, DS, RPS and ASG contributed towards the analysis and interpretation of the observations. DS prepared final draft of manuscript. SG associated with draft editing and writing. All authors contributed to the discussion of the results.

Declarations

Conflict of Interests It is declared that the authors have no known competing financial interests or personal relationships that could have appeared to influence the work reported in this paper.

References

Ambade B, Sankar TK, Panicker AS, Gautam AS, Gautam S (2021) Characterization, seasonal variation, source apportionment and health risk assessment of black carbon over an urban region of East India. Urban Clim 38:100896

Asmi E, Frey A, Virkkula A, Ehn M, Manninen HE, Timonen H, Tolonen-Kivimaki O, Aurela M (2010) Hillamo R and Kulmala M 2010 Hygroscopicity and chemical composition of Antarctic sub-micrometre aerosol particles and observations of new particle formation. Atmos Chem Phys 10:4253–4271. https://doi.org/10.5194/acp-10-4253-2010

Betha R, Spracklen DV, Balasubramanian R (2013) Observations of new aerosol particle formation in a tropical urban atmosphere. Atmos Environ 71:340–351

Blanchard DC (1963) Electrification of the atmosphere by particles from bubbles in the sea. Prog Oceanogr 1:71–202

Bonn B, Boy M, Kulmala M, Groth A, Trawny K, Borchert S, Jacobi S (2009) A new parametrization for ambient particle formation over coniferous forests and its potential implications for the future. Atmos Chem Phys 9:8079–8090. www.atmos-chem-phys.net/9/8079/2009/

Boy M, Kulmala M (2002) Nucleation events in the continental boundary layer: influence of physical and meteorological parameters. Atmos Chem Phys 2:1–16. https://doi.org/10.5194/acp-2-1-2002

Bricard J (1965) Action of radioactivity and of pollution upon parameters of atmospheric electricity. In: Coroniti SC (ed) Problems of atmospheric and space electricity. Elsevier Science, New York, pp 87–109

Carslaw KS, Harrison RG, Kirkby J (2002) Cosmic rays, clouds, and climate. Science 298:1732–1737

Chalmers JA (1967) Atmospheric electricity. Pergamon Press, London

Chen X, Paatero J, Kerminen V-M, Riuttanen L, Hatakka J, Hiltunen V, Paasonen P, Hirsikko A, Franchin A, Manninen HE, Petäjä T, Viisanen Y, Kulmala M (2016a) Responses of the atmospheric concentration of radon-222 to the vertical mixing and spatial transportation. Boreal Environ Res 21:299–318

Chen X, Kerminen V-M, Paatero J, Paasonen P, Manninen HE, Nieminen T, Petäjä T, Kulmala M (2016b) How do air ions reflect variations in ionizing radiation in the lower atmosphere in a Boreal forest? Atmos Chem Phys 16:14297–14315. https://doi.org/10.5194/acp-16-14297-2016

Clement CF, Pirjola L, dal Maso M, Mäkelä JM, Kulmala M (2001) Analysis of particle formation bursts observed in Finland. J Aerosol Sci 32:217–236

Cobb WE (1977) Atmospheric electric measurements at the south pole. In: Dolezalek H, Reiter R, Steinkopff D (eds) Electrical processes in atmospheres. Federal Republic of Germany, pp 161–167

Dal Maso M, Kulmala M, Riipinen I, Wagner R, Hussein T, Aalto PP, Lehtinen KEJ (2005) Formation and growth of fresh atmospheric aerosols: eight years of aerosol size distribution data from SMEAR II, Hyytial¨ a, Finland. Boreal Environ Res 10:323–336

Dhanorkar S, Kamra AK (1991) Measurement of mobility spectrum and concentration of all atmospheric ions with a single apparatus. J Geophys Res 91:18671–18678

Dhanorkar S, Kamra AK (1993a) Diurnal variations of the mobility spectrum of ions and size distribution of fine aerosols in the atmosphere. J Geophys Res 98:2639–2650. https://doi.org/10.1029/92JD02545

Dhanorkar S, Kamra AK (1993b) Diurnal and seasonal variations of the small-, intermediate-, and large-ion concentrations and their contributions to polar conductivity. J Geophys Res 98:14895–14908. https://doi.org/10.1029/93JD00464

Dinoi A, Weinhold K, Weidensohler A, Contini D (2021) Study of new particle formation events in Southern Italy. Atmos Environ 244:117920

Gautam S, Brema J (2020) Spatio-temporal variation in the concentration of atmospheric particulate matter: a study in fourth largest

urban agglomeration in India. Environ Technol Innov. https://doi.org/10.1016/j.eti.2019.100546
Gautam AS, Siingh D, Kamra AK (2017) Statistical analysis of the atmospheric ion concentrations and mobility distributions at a tropical station, Pune. Q J R Meteorol Sco 143:2116–2128. https://doi.org/10.1002/qj.3071
Gautam S, Gautam AS, Singh K, James EJ, Brema J (2021) Investigations on the relationship among lightning, aerosol concentration, and meteorological parameters with specific reference to the wet and hot humid tropical zone of the southern parts of India. Environ Technol Innov. https://doi.org/10.1016/j.eti.2021.101414
Gautam AS (2017) generation mechanisms and characteristics of air ions at a tropical station, Ph.D. thesis, Savitribai Phule Pune University, Pune
Gollakota ARK, Gautam S, Santosh M, Sudan HA, Gandhi R, Jebadurai VS, Shu CM (2021) Bioaerosols: characterization, pathways, sampling strategies, and challenges to geo-environment and health. Gondwana Res 99:178–203
Gonser SG, Klein F, Birmile W, Gorob J, Kulmal M, Manninen HE, Wieldensohler A, Held A (2014) Ion–particle interactions during formation and growth at a coniferous forest site in Central Europe. Atmos Chem Phys 14:10547–10563
Gopalakrishnan V, Pawar SD, Siingh D, Kamra AK (2005) Intermediate ion formation in the ship's exhaust. Geophys Res Lett 32:L11806. https://doi.org/10.1029/2005GL022613
Green AES, Jackman CH, Garvey RH (1977) Electron impact on atmospheric gases. II—yield spectra. J Geophys Res 82:5104–5111. https://doi.org/10.1029/JA082i032p05104
Hensen A, van der Hage JCH (1994) Parameterization of cosmic radiation at sea level. J Geophys Res 99:10693–10695
Hirsikko A, Laakso L, Hõrrak U, Aalto PP, Kerminen V-M, Kulmala M (2005) Annual and size dependent variation of growth rates and ion concentrations in Boreal forest. Boreal Environ Res 10:357–369
Hoppel WA (1985) Ion–aerosol attachment coefficients, ion depletion, and the charge distribution on aerosols. J Geophys Res 90:5917–5923
Hoppel WA, Frick GM (1986) Ion–aerosol attachment coefficient and the steady state charge distribution on aerosol in a bipolar environment. J Aerosol Sci 5:1–21
Hoppel WA, Fitzgerald JW, Frick GM, Larson R, Mack EJ (1990) Aerosol size distributions and optical properties found in the marine boundary layer over the Atlantic Ocean. J Geophys Res 95:3659–3686. https://doi.org/10.1029/JD095iD04p03659
Hoppel WA, Anderson RV, Willett JC (1986) Atmospheric electricity in the planetary boundary layer. In: The Earth's electrical environment. National Academy Press, Washington, DC, pp 149–165
Horrak U, Salm J, Tammet H (1998) Bursts of intermediate ions in atmospheric air. J Geophys Res 103:13909–13915
Horrak U, Salm J, Tammet H (2000) Statistical characterization of air ion mobility spectra at Tahkuse Observatory: classification of air ions. J Geophys Res 105:9291–9302
Horrak U, Salm J, Tammet H (2003) Diurnal variation in the concentration of air ions of different mobility classes in a rural area. J Geophys Res 108:4653. https://doi.org/10.1029/2002JD003240
Horrak U, Tammet H, Aalto PP, Vana M, Hirsikko A, Laakso L, Kulmala M (2006) Formation of charged nanometer aerosol particles associated with rainfall: atmospheric measurements and lab experiment. Rep Ser Aerosol Sci 80:180–185
Horrak U (2001) Air ion mobility spectrum at a rural area. Ph.D. Thesis, University of Tartu, Tartu, Estonia
Huang X, Zhou L, Ding A, Qi X, Nie W, Wang M, Chi X, Petaja T, Kerminen V-M, Roldin P, Rusanen A, Kulmala M, Boy M (2016) Comprehensive modelling study on observed new particle formation at the SORPES station in Nanjing, China. Atmos Chem Phys 16:2477–2492. https://doi.org/10.5194/acp-16-2477-2016
Jaenicke R (1984) Our knowledge about the atmospheric aerosol. In: Proceedings of the 11th international conference on atmospheric aerosols, condensation and ice nuclei, vol 1. Hungadan Meteorology Service, Budapest, pp 99–107
Kamra AK, Gautam AS, Siingh D (2015a) Charged nanoparticles produced by splashing of raindrops. J Geophys Res 120:6669–6681. https://doi.org/10.1002/2015JD023320
Kamra AK, Siingh D, Gautam AS, Kanawade VP, Tripathi SN, Srivastava AK (2015b) Atmospheric ions and new particle formation events at a tropical location, Pune, India. Q J R Meteorol Soc 141:3140–3156. https://doi.org/10.1002/qj.2598
Kamsali N, Prasad BSN, Chandrashekara MS, Paramesh L, Madhava MS, Sannappa J, Pawar SD, Murugavel P, Kamra AK (2003) Radon and its short-lived progeny: variations near the ground. Radiat Meas 36:413–417
Kanawade V, Tripathi SN (2006) Evidence for the role of ion-induced particle formation during an atmospheric nucleation event observed in Tropospheric Ozone Production about the Spring Equinox (TOPSE). J Geophys Res 111:D02209. https://doi.org/10.1029/2005JD006366
Kanawade VP, Tripathi SN, Siingh D, Gautam AS, Srivastava AK, Kamra AK, Soni VK, Sethi V (2014) Observations of new particle formation at two distinct Indian subcontinental urban locations. Atmos Environ 96:370–379. https://doi.org/10.1016/j.atmosenv.2014.08.001
Kataoka T, Yunoki E, Shimizu M, Mori T, Tsukamoto O, Ohhashi Y, Sahashi K, Maitani T, Miyashita K, Fujikawa Y, Kudo A (1998) Diurnal variation in radon concentration and mixing-layer depth. Bound Layer Meteorol 89:225–250
Kojima H (1984) Relation between intermediate ions and meteorological factors. Res Lett Atmos Electr 4:49–53
Kolarz P, Gaisberger M, Madl P, Hofmann W, Ritter M, Hartl A (2012) Characterization of ions at Alpine waterfalls. Atmos Chem Phys 12:3687–3697. https://doi.org/10.5194/acp-12-3687-2012
Kulmala M, Toivonen A, Mäkelä JM, Laaksonen A (1998) Analysis of the growth of nucleation mode particles observed in Boreal forest. Tellus B 50:449–462
Kulmala M, Vehkamaki H, Petaja T, Dal Maso M, Lauri A, Kerminen VM, Birmili W, McMurry PH (2004) Formation and growth rates of ultrafine atmospheric particles: a review of observations. J Aerosol Sci 35:143–176
Kulmala M, Lehtinen KEJ, Laaksonen A (2006) Cluster activation theory as an explanation of the linear dependence between formation rate of 3 nm particles and sulphuric acid concentration. Atmos Chem Phys 6:787–793. https://doi.org/10.5194/acp-6-787-2006
Kulmala M et al (2013) Direct observations of atmospheric aerosol nucleation. Science 339:943–946
Kumar S, Siingh D, Singh RP, Singh AK, Kamra AK (2018) Lightning discharges, cosmic rays and climate. Surv Geophys 39:861–899. https://doi.org/10.1007/s10712-018-9469-z
Laakso L, Petäjä T, Lehtinen KEJ, Kulmala M, Paatero J, Hõrrak U, Tammet H, Joutsensaari J (2004) Ion production rate in a Boreal forest based on ion, particle and radiation measurements. Atmos Chem Phys 4:1933–1943
Lee X, Gao Z, Zhang C, Chen C, Hu Y, Jain W, Liu S, Lu L, Sun J, Wang J, Zeng Z, Zhang Q, Zhao M, Zhou M (2015) Priorities for boundary–layer meteorology research in China. Bull Am Meterol Soc 96:149–151
Mäkelä J, Dal Maso M, Pirjola L, Keronen P, Laakso L, Kulmala M, Laaksonen A (2000) Charactristics of the atmospheric particle formation events observed at a Boreal forest site in southern Finland. Boreal Environ Res 5:299–313
Mirme S, Mirme A (2013) The mathematical principles and design of the NAIS – a spectrometer for the measurement of cluster

ion and nanometer aerosol size distributions. Atmos Meas Tech 6:1061–1071
Mirme A et al (2007) A wide-range multi-channel air ion spectrometer. Boreal Environ Res 12:247–264
Misaki M (1964) Mobility spectrums of large ions in the New Mexico semi desert. J Geophys Res 69:3309–3318
Nilsson ED, Rannik Ü, Kulmala M, Buzorius G, O'dowd CD (2001a) Effects of continental boundary layer evolution, convection, turbulence and entrainment, on aerosol formation. Tellus B 53:441–461. https://doi.org/10.1034/j.1600-0889.2001.530409.x
Nilsson ED, Paatero J, Boy M (2001b) Effects of air masses and synoptic weather on aerosol formation in the continental boundary layer. Tellus B 53:462–478
O'Dowd CD, Aalto P, Hameri K, Kulmala M, Hoffmann T (2002a) Atmospheric particles from organic vapours. Nature 416:497–498
O'Dowd CD, Jimenez JL, Bahreini R, Flagan RC, Seinfeld JH, Pirjola L, Kulmala M, Jennings SG, Hoffmann T (2002b) Marine particle formation from biogenic iodine emissions. Nature 417:632–636
Pal S, Lee TR, Phelps S, De Wekker SF (2014) Impact of atmospheric boundary layer depth variability and wind reversal on the diurnal variability of aerosol concentration at a valley site. Sci Total Environ 496:424–434
Porstendorfer J (1994) Properties and behavior of Radon and thorn and their decay products in the air. J Aerosol Sci 25:219–263
Qian S, Sakurai H, McMurry PH (2007) Characteristics of regional nucleation events in urban East St. Louis. Atmos Environ 41:4119–4127
Salm J, Tammet H, Iher H, Horrak U (1992) The dependence of small air ion mobility spectra in the ground layer of the atmosphere on temperature and pressure. Acta Comment Univ Tartu 947:50–56
Schumann RR, Owen DE, Asher-Bolinder S (1988) Weather factors affecting soil gas radon concentrations at a single site in the semi-arid western US. In: Osborne MC, Harrison J (eds) Proceedings of the 1988 E.P.A. symposium on radon and radon reduction technology, vol 2. Poster presentation. Environmental Protection Agency Publication, 600/9-89-00613, p 3-1–3-13
Siingh D, Singh RP (2010) The role of cosmic rays in the Earth's atmospheric processes. Pramana J Phys 74:153–168. https://doi.org/10.1007/s12043-010-0017-8
Siingh D, Pawar SD, Gopalakrishnan V, Kamra AK (2005) Measurements of the ion concentrations and conductivity over the Arabian Sea during the ARMEX. J Geophys Res 110:D18207. https://doi.org/10.1029/2005JD005765
Siingh D, Gopalakrishnan V, Singh RP, Kamra AK, Singh S, Pant V, Singh R, Singh AK (2007a) Atmospheric global electric circuit: an overview. Atmos Res 84:91–110
Siingh D, Pant V, Kamra AK (2007b) b Measurements of positive ions and air-Earth current density at Maitri, Antarctica. J Geophys Res 112:D13212. https://doi.org/10.1029/2006JD008101
Siingh D, Pant V, Kamra AK (2011) The ion–aerosol interaction from the ion mobility and aerosol particle size distribution measurements on January 17 and February 18 2005 at Maitri, Antarctica—a case study. J Earth Syst Sci 120:735–754
Siingh D, Pant V, Kamra AK (2013a) Temperature-dependence of the positive intermediate ion concentrations at Maitri, Antarctica. J Atmos Solar Terr Phys 104:67–74
Siingh D, Gautam AS, Kamra AK, Komsaare K (2013b) Nucleation events for the formation of charged aerosol particles at a tropical station-preliminary results. Atmos Res 132–133:239–252. https://doi.org/10.1016/j/atmosres.2013.05.024
Siingh D, Singh RP, Gopalakrishnan V, Singh RP (2013c) Fair-weather atmospheric electricity study at Maitri (Antarctica). Earth Planet Space 65:1541–1553. https://doi.org/10.5047/eps.2013.09.011
Siingh D, Gautam AS, Buchunde PS, Kamra AK (2018) Classification of the new particle formation events observed at a tropical site, Pune, India. Atmos Environ 190:10–22. https://doi.org/10.1016/j.atmosenv.2018.07.025
Singh AK, Siingh D, Singh RP (2011) Impact of galactic cosmic rays on Earth's atmosphere and human health. Atmos Environ 45:3806–3818. https://doi.org/10.1016/j.atmosenv.2011.04.027
Sullivan RC, Crippa P, Matsui H, Leung LR, Zhao C, Thota A, Pryor SC (2018) New particle formation leads to cloud dimming. Npj Clim Atmos Sci 1:9. https://doi.org/10.1038/s41612-018-0019-7
Tammet H (1995) Size and mobility of nanometer particles, clusters and ions. J Aerosol Sci 26:459–475
Tammet H (1998) Reduction of air ion mobility to standard conditions. J Geophys Res 103:13933–13937
Tammet H, Horrak U, Laakso L, Kulmala M (2006) Factors of air ion balance in a coniferous forest according to measurements in Hyytiala, Finland. Atmos Chem Phys 6:3377–3390. https://doi.org/10.5194/acp-6-3377-2006
Tammet H, Komsaare K, Hõrrak U (2014) Intermediate ions in the atmosphere. Atmos Res 135–136:263–273. https://doi.org/10.1016/j.atmosres.2012.09.009
Vehkamaki H (2006) Classical nucleation theory in multicomnent systems. Springer, Berlin, pp 176. doi: https://doi.org/10.1007/3-540-31218-8
Victor NJ, Siingh D, Singh RP, Singh R, Kamra AK (2019) Diurnal and seasonal variations of Radon (222Rn) and their dependence on soil moisture and vertical stability of the lower atmosphere at Pune. India J Atmos Solar Terr Phys 195:105–118. https://doi.org/10.1016/j.jastp.2019.105118
Wagner R, Manninen HE, Franchin A, Lehtipalo K, Mirme S, Steiner G, Petäjä T, Kulmala M (2016) On the accuracy of ion measurements using a neutral cluster and air ion spectrometer. Boreal Environ Res 21:230–241
Waring MS, Wells JR, Siegel JA (2011) Secondary organic aerosol formation from ozone reactions with single terpenoids and terpenoid mixtures. Atmos Environ 45:4235–4242
Weber RJ, Marti JJ, McMurry PH, Eisele FL, Tanner DJ, Jefferson A (1997) Measurements of new particle formation and ultrafine particle growth rates at a clean continental site. J Geophys Res 102:4375–4385
Wilson CTR (1924) The electric field of a thundercloud and some of its effects. Proc Phys Soc Lond 37:32D. https://doi.org/10.1088/1478-7814/37/1/314
Yu F (2007) Improved quasi-unary nucleation model for binary $H2SO_4$-H_2O homogeneous nucleation. J Chem Phys 127:054301
Yu F (2010) Ion-mediated nucleation in the atmosphere: key controlling parameters, implications, and look-up table. J Geophys Res 115:D03206. https://doi.org/10.1029/2009JD012630
Yu F, Turco RP (2000) Ultrafine aerosol formation via ion-mediated nucleation. Geophys Res Lett 27:883–886. https://doi.org/10.1029/1999GL011151
Yu F, Turco RP (2001) From molecular clusters to nanoparticles: role of ambient ionization in tropospheric aerosol formation. J Geophys Res 106:4797–4814. https://doi.org/10.1029/2000JD900539
Yu F, Turco RP (2008) Case studies of particle formation events observed in Boreal forests: implications for nucleation mechanisms. Atmos Chem Phys 8:6085–6102
Yu F, Turco RP (2011) The size-dependent charge fraction of sub-3-nm particles as a key diagnostic of competitive nucleation mechanisms under atmospheric conditions. Atmos Chem Phys 11:9451–9463
Yu F, Wang Z, Luo G, Turco RP (2008) Ion-mediated nucleation as an important global source of tropospheric aerosols. Atmos Chem Phys 8:2537–2554
Yu F, Luo G, Bates T, Anderson B, Clarke A, Kapustin V, Yantosca R, Wang Y, Wu S (2010) Spatial distributions of particle number concentrations in the global troposphere: simulations, observations, and implications for nucleation mechanisms. J Geophys Res 115:D17205. https://doi.org/10.1029/2009JD013473